IFSCC 2025 full paper (IFSCC2025-1326)

"Development of TA-GNR@TiO_2 Core@Shell Composites for IR-A Blocking Cosmetics"

Yu Ra Lim [1], Yeong Jun Jeon [1], Ji Won Choi [2], Hyo-won Han [2], Da Sol Song [3], Hyo Hyun Kim [3], Yong Woo Kim [3], Young Hoon Cho [3], and Eue-soon Jang [1,2]*

[1] Department of Applied Chemistry, Kumoh National Institute of Technology, Gumi, Gyeongbuk, South Korea; [2] Golden Crow Co. Ltd., #140 Global building, Gumi, Gyeongbuk, South Korea; [3] R&D Center, Kolmar Korea, Seoul, 06800, South Korea

1. Introduction

Infrared (IR) radiation can be categorized into three types depending on the wavelength ranges, which are near-IR (IR-A, 700–1400 nm), mid-IR (IR-B, 1400–3000 nm), and distant-IR (IR-C, 3000–1 mm). The presence of water molecules in the Earth's atmosphere has a notable impact on the intensity of IR radiation reaching the surface of the planet. The absorption of IR radiation by water molecules, particularly in the IR-B and IR-C ranges, leads to a considerable reduction in the strength of the radiation when it reaches the Earth's surface [1,2]. By contrast, IR-A radiation with a higher energy has a lower probability of being absorbed by the vibrational modes of the water molecules owing to the principles of quantum physics. Consequently, IR-A radiation reaching the Earth's surface exhibits a lower attenuating effect than IR-B and IR-C radiation [1]; moreover, this phenomenon is equally applicable to the human body. On an average, skin accounts for approximately 18–20% of the total water content of the body [2]. When exposed to solar radiation, IR-B and IR-C radiation do not deeply penetrate the skin owing to water absorption in the skin; however, over 65% of the IR-A radiation reaches the dermis and subcutaneous layers [1,3]. IR-A is absorbed by cytochrome *c* oxidase in the mitochondrial respiratory chain, leading to an increased production of adenosine triphosphate (ATP) in the mitochondria [1,4]. This increase in the intracellular ATP levels has potential therapeutic benefits in the treatment of various diseases [5]. However, prolonged exposure of the skin to IR-A can trigger the production of matrix metalloproteinases (MMPs) through the generation of reactive oxygen species (ROS) owing to the thermal stress caused by an increase in the skin temperature [6], which is the main mechanism responsible for thermal aging. Shimizu et al. reported that repeated exposure to IR-A not only induces a reduction in the thickening of the epidermal cell layer but also an increase in the thickness of the stratum corneum in human skin [7]. This indicates that repeated IR-A exposure may negatively affect skin aging. Therefore, the development of skincare products that can mitigate the negative effects of IR-A radiation on human skin is an important research area. Novel materials for use in cosmetics that are biologically safe and can scatter or absorb IR-A radiation must be developed to protect the skin. However, most materials with bandgap energies corresponding to the

IR-A wavelengths (0.89–1.77 eV), such as InP, GaSb, GaInSb, GaAs, and CdTe, pose cytotoxicity issues, making them unsuitable for cosmetic applications [8,9]. By contrast, gold nanorods (GNRs) exhibit surface plasmon resonance (SPR) in the longitudinal direction at IR-A wavelengths [10]. As the aspect ratio of the GNR increases, the absorption wavelength of the longitudinal SPR (LSPR) undergoes a red shift [11]. In our previous study, we demonstrated that a sunscreen containing a mixture of GNRs and TiO_2 powder could reduce the generation of reactive oxygen species (ROS) and matrix metallopeptidase-1 (MMP-1) by blocking IR-A radiation. In this study, we successfully synthesized a GNR@TiO_2 core@shell composite to create a more effective IR-A blocking cosmetic formulation. Moreover, the surface of the GNR@TiO_2 was modified with tannic acid (TA) to reduce the photocatalytic effect of the TiO_2 layer. To evaluate the thermal blocking efficiency of the TA-GNR@TiO_2 composite formulation in comparison with the GNR-based cream, in-vitro tests and a clinical study were conducted.

2. Materials and Methods

2.1 Chemical and reagents

Cetyltrimethylammonium bromide (CTAB; ≥99%), gold(III) chloride trihydrate ($HAuCl_4 \cdot 3H_2O$; ≥99.9%), sodium tetrahydridoborate ($NaBH_4$; ≥98.0%), silver nitrate ($AgNO_3$; ≥99.0%), L-ascorbic acid (AA; ≥99.0%), sodium citrate dihydrate, sodium bicarbonate ($NaHCO_3$), Poly(sodium 4-styrenesulfonate) (PSS), and titanium(III) chloride solution (15% $TiCl_3$, 10% HCL) were purchased from Sigma-Aldrich (USA). Sodium dodecyl sulfate (SDS) was purchased from Wako Pure Chemical Co. (Japan). Tannic acid was purchased from Samchun Chemical (Korea). The TiO_2 nanoparticles (Tayca, Japan) were provided by Kolmar (Korea). Dulbecco's Modified Eagle Medium (DMEM, 4500 mg/L glucose), Iscove's Modified Dulbecco's medium (IMDM, 1000 mg/L glucose), Phosphate-buffered saline (PBS, pH 7.4) solution, and Fetal Bovine Serum (FBS) were purchased from Welgene Korea. The 2′,7′-dichlorodihydrofluorescein diacetate (H_2DCFDA) and 3-(4,5)-dimethylthiazol-2-yl-2,5-diphenyltetrazolium bromide (MTT) were purchased from Invitrogen (USA) and AMRESCO LLC, respectively. The CCD-986sk (human fibroblast) and HaCaT (human keratinocyte) cell lines were provided by the Korean Cell Line and American Type Culture Collection (ATCC).

2.2 Synthesis of TA-GNR@TiO_2 core@shell composites

Gold nanorods (GNRs) were synthesized following a previously reported procedure [12]. The Au seed solution was prepared by mixing 0.1 mL of 25 mM $HAuCl_4 \cdot 3H_2O$ with 10 mL of 0.1 M CTAB. Subsequently, 0.6 mL of ice-cold 0.1 M $NaBH_4$ was rapidly added under vigorous vortexing for 3 minutes, yielding a brownish-yellow Au seed solution. This solution was aged at room temperature for 30 minutes before use. The growth solution was prepared by mixing 1L of 0.05 M CTAB, 20 mL of 25 mM $HAuCl_4$, 4.8 mL of 0.1 M L-ascorbic acid (AA), 10 mL of 10 mM $AgNO_3$ aqueous solutions. The resulting growth solution was stirred at 35 °C until it became colorless. Then, 0.8 mL of the Au seed solution was sequentially added to the growth solution. The final mixture was allowed to react at 35 °C for 12 hours. The as-prepared GNR solution was purified by repeated centrifugation and dispersed in 100 mL of deionized (DI) water. To reduce the cytotoxicity, the CTAB on the GNR surface was substituted by citrate anions through Mehtala's procedure [13]. In brief, 0.2473 g of PSS was added to 100 mL of a 500 ppm GNR solution and the solution was stirred for overnight at room temperature. The resulting PSS-GNRs were collected *via* centrifugation and redispersed in 8.4 mM sodium citrate dihydrate solution, then stirred overnight at room temperature. Finally, the citrate modified-GNR solution was purified by two washing steps and dispersed in DI water for storage.

To fabricate GNR@TiO_2 core-shell composites, a TiO_2 layer was formed on the GNR surface via a hydrolysis reaction of a $TiCl_3$ under acidic conditions. To render the GNR surface negatively charged, 400 mL of 150 ppm GNR solution was mixed with 400 mL of 0.2 M SDS

solution and stirred for 30 minutes. The resulting solution was washed twice with DI water and redispersed in 75 mL of DI water. For the TiO_2 precursor solution, 50 mL of $TiCl_3$ solution was added to 1 L of DI water, and the pH was adjusted to 2.5 using 1 M $NaHCO_3$ solution. The entire volume of the SDS-coated GNR solution was rapidly added and stirred at room temperature for 30 minutes. The synthesized GNR@TiO_2 composites were washed twice with ethanol by centrifugation and redispersed in DI water. Tannic acid-coated GNR@TiO_2 composites (TA-GNR@TiO_2) were synthesized by adding 2 mL of 15 mM TA to 190 mL of 80 ppm Au GNR@TiO_2 solution, followed by stirring for 3 hours. After completion of the reaction, the TA-GNR@TiO_2 solution was washed twice with DI water and redispersed in DI water.

2.3 Characterization

The ultraviolet–visible (UV–Vis) absorption spectra of the as-prepared products were obtained by using a Shimadzu UV-2600 spectrophotometer (Tokyo, Japan). The morphologies and particle size distributions of the final products were confirmed by using transmission electron microscopy (TEM) combined with energy-dispersive X-ray (EDX) spectroscopy and 90Plus particle size and zeta analyzer (Brookhaven, NY, USA). The samples were also studied by powder X-ray diffraction (XRD; SWXD-D-MAX/2500-PC, Japan) patterns, Fourier-transform infrared spectroscopy (FTIR; Thermo Scientific Nicolet iS5, USA), and atomic absorption spectroscopy (AAS; MegaA-700FG, Korea) measurements.

2.4 Preparation of sunscreen

To formulate the cream-based sunscreen, the vehicle and the as-prepared products were uniformly dispersed and mixed using a homogenizer.

Role	Ingredients
Solvent	Water, Propanediol, Butylene Glycol, Pentylene Glycol, 1,2-Hexanediol
Oils and emollients	Caprylic/ Capric Triglyceride, Coco-Caprylate/ Caprate, Dimethicone, Candelilla/ Jojoba/ Rice Bran Polyglyceryl-3 Esters
Viscosity modifiers and stabilizers	Cetearyl Alcohol, Polyacrylate Crosspolymer-6, Ammonium Acryloyldimethyltaurate/VP Copolymer
Emulsifiers	Polyglyceryl-3 Distearate, Polyglyceryl-6 Distearate, Glyceryl Stearate Citrate, Sodium Stearoyl Glutamate, Polysorbate 60
Fillers and texture enhancers	Silica, Polymethylsilsesquioxane
Protective and stabilizing coatings	Triethoxycaprylylsilane

2.5 In-vitro cytotoxicity

Cytotoxicity of GNR@TiO_2 and TA-GNR@TiO_2 was evaluated using an MTT assay on HaCaT cells (human keratinocyte cell line). HaCaT cells were seeded in 96-well culture plates at a density of 2×10^4 cells/well and incubated for 24 hours at 37 °C with 5% CO_2. Subsequently, GNR@TiO_2 and TA-GNR@TiO_2 at various concentrations (0 ~ 300 μg Au/mL) were added and incubated for 12 hours. The percentage of cell viability was determined at 570 nm using an ELISA plate reader (BioTek, Winooski, VT, USA).

To assess the cell viability under UV light transmitted through the cream, an MTT assay was performed on BLO-11 cells (mouse fibroblast cell line). BLO-11 cells were seeded in 48-well culture plates at a density of 2.5×10^4 cells/well and incubated for 12 hours at 37 °C with 5% CO_2. Subsequently, cream containing TiO_2, GNR, or TA-GNR@TiO_2 was evenly applied to the lid of the cell culture plate at a concentration of 5 mg/cm². After irradiation with a UV lamp at an intensity of 1.77 mW/cm² for 90 minutes, the percentage of cell viability was determined at 570 nm using an ELISA plate reader (BioTek, Winooski, VT, USA).

2.6 Photocatalytic activity

To compare the photocatalytic performance of GNR@TiO_2 and TA-GNR@TiO_2 under UV irradiation, aqueous suspensions of both materials were prepared, each containing 10 ppm methylene blue (MB) and 30 ppm Au. These suspensions were then exposed to UV light at an

intensity of 1.77 mW/cm^2, and the photocatalytic degradation of MB was monitored by measuring the absorbance of the solutions at 30-minute intervals using a UV-Vis spectrophotometer.

2.7 Evaluation of reactive oxygen species (ROS) generation by DCF-DA staining

To assess ROS generation resulting from the near-infrared blocking effect of TA-GNR@TiO_2, CCD-986sk (human fibroblast ,1 x 10^5 cells/dish) cells were cultured in Cell culture dishes (Φ 35 × 10 ㎜) for 5 days at 37 °C and 5% CO_2. Subsequently, a TA-GNR@TiO_2 cream (5 mg/cm²) was applied to the dish lids, and the cells were irradiated with near-infrared light for 30 minutes from a distance of 25 cm. Following irradiation, ROS production was evaluated by staining the cells with the fluorescent indicator DCF-DA.

2.8 IR-A blocking evaluation

Scheme 1 illustrates the in-vitro testing method for IR-A blocking. A commercially available IR lamp (250 W, Philips, Netherlands) was used as the light source for the in-vitro IR-A blocking test. By measuring the intensity of the IR lamp at a distance of 25 cm using a digital optical power meter, the power densities at wavelengths of 780, 960, and 1,061 nm were found to be 51.3, 34.5, and 77.6 mW/cm^2, respectively. These IR-A power densities of the IR lamp are more than twice as strong as the IR-A intensity reaching the Earth's surface.

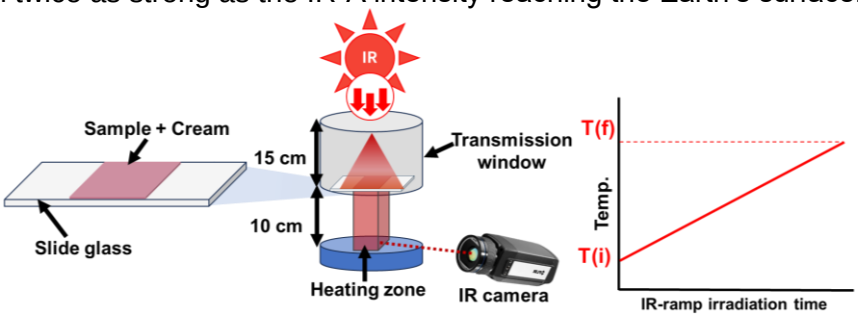

Scheme 1. Schematic of the in-vitro test for IR-A blocking.

$$\Delta T = T_f - T_i \quad \cdots\cdots\cdots\cdots\cdots\cdots\cdots\cdots\cdots\cdots\cdots\cdots\cdots\cdots\cdots\cdots\cdots\cdots\cdots\cdots (1)$$

$$TRI_{sample}(\%) = \frac{\Delta T_{glass} - \Delta T_{sample}}{\Delta T_{glass}} \times 100(\%) \quad \cdots\cdots\cdots\cdots\cdots\cdots\cdots\cdots\cdots (2)$$

$$TRI_{vehicle}(\%) = \frac{\Delta T_{glass} - \Delta T_{vehicle}}{\Delta T_{glass}} \times 100(\%) \quad \cdots\cdots\cdots\cdots\cdots\cdots\cdots\cdots\cdots (3)$$

$$\Delta TRI(Temperature\ Rise\ Inhibition, \%) = TRI_{sample} - TRI_{vehicle} \quad \cdots\cdots\cdots (4)$$

To evaluate IR-A blocking performance, cream was uniformly applied to a slide glass at a density of 5 mg/cm². The cream-coated slide glass was vertically mounted 15 cm away from the IR lamp, allowing IR light to transmit through it. To measure the increasing temperature *via* transmitted IR light, a rubber-covered petri dish serving as the heating zone was placed 10 cm below the slide glass as shown in the Scheme 1. The rubber surface of the petri dish was heated by irradiating it with the transmitted IR light for 20 minutes, and the surface temperature of the heating zone was measured using an IR camera. The measured temperature values recorded in the heating zone were used to calculate the temperature rise inhibition (TRI) percentages for the vehicle and sample creams using Equations (1-3), respectively [14]. Subsequently, Equation (3) was employed to calculate the change in the temperature rise inhibition rate (ΔTRI) of the sample cream compared to that of the vehicle cream [14].

2.9 Clinical trials for evaluation of thermal blocking efficiency

The clinical trial was commissioned to the Korean Dermatological Research Institute and conducted with 40 subjects selected as shown in Table 1 (IRB Approval No.: KDRI-IRB-240928). Group 1 (n = 20) underwent efficacy evaluation of the GNR (300 ppm Au) containing cream, and Group 2 (n = 20) underwent efficacy evaluation of the TA-GNR@TiO_2 (300 ppm Au) containing cream.

Group 1	No.	ID	Age	Gender	No.	ID	Age	Gender
GNR(300 ppm) + TiO_2(10^5 ppm)	1	2273	39	Female	11	2689	52	Female
	2	2588	40	Female	12	1096	54	Female
	3	6782	43	Female	13	4359	54	Female
	4	2823	45	Female	14	3371	54	Female
	5	7615	46	Female	15	731	55	Female
	6	4443	46	Female	16	1965	56	Female
	7	6690	47	Female	17	7515	56	Female
	8	6842	48	Female	18	2470	57	Female
	9	2539	49	Female	19	3648	58	Female
	10	1749	51	Female	20	5205	60	Female

Group 2	No.	ID	Age	Gender	No.	ID	Age	Gender
GNR@TiO_2(300 ppm) + TiO_2(10^5 ppm)	1	5020	30	Male	11	6149	49	Female
	2	7648	31	Male	12	4033	50	Female
	3	6562	38	Male	13	3113	50	Female
	4	307	38	Female	14	1854	51	Female
	5	172	40	Female	15	5268	51	Female
	6	7272	41	Male	16	2118	53	Female
	7	3153	45	Female	17	3594	55	Female
	8	6347	46	Female	18	4303	56	Female
	9	2379	47	Female	19	5376	57	Female
	10	4167	48	Female	20	6321	59	Female

Table 1. Basic information of study participants by samples and schematic diagram of sample application method.

The test method involved applying 2 mg/cm² of each cream (vehicle, TiO_2 (10^5 ppm) cream, sample (GNR or TA-GNR@TiO_2 (300 ppm Au) + TiO_2 (10^5 ppm) cream) to the test area (dorsum) with a distance of 5 cm. Subsequently, the sites were irradiated with an infrared irradiator (INFRALUX-300, λ = 780 ~ 1400 nm, Daekyung Electronics Co. Ltd., Republic of Korea) for 10 minutes, and skin temperature changes were measured using an IR camera (FLIR T-420, USA) during this irradiation period. The collected data were analyzed for statistical significance using the Minitab 19 program (Minitab®19.2, Minitab Inc., USA). Throughout the trial period, a dermatologist monitored the occurrence of any adverse reactions due to sample use (erythema, edema, scaling, itching, stinging, burning sensation, and other abnormalities) to ensure the safe conduct of the clinical trial.

3. Results and discussion

3.1 Characterization of materials

As shown in Fig. 1(a), the GNRs exhibit good uniformity with an average length of 80 ± 4 nm and an average width of 18 ± 2 nm. TEM image of GNR core with TiO_2 shell (GNR@TiO_2) is shown in Fig. 1(b), confirming the formation of uniform TiO_2 coating with averaged shell thicknesses of 67.1 ± 13.7 nm. Compared to the nanometer-scale GNRs, the micro-sized GNR@TiO_2 composites can circumvent the regulatory concerns associated with nanoparticles in cosmetic products.

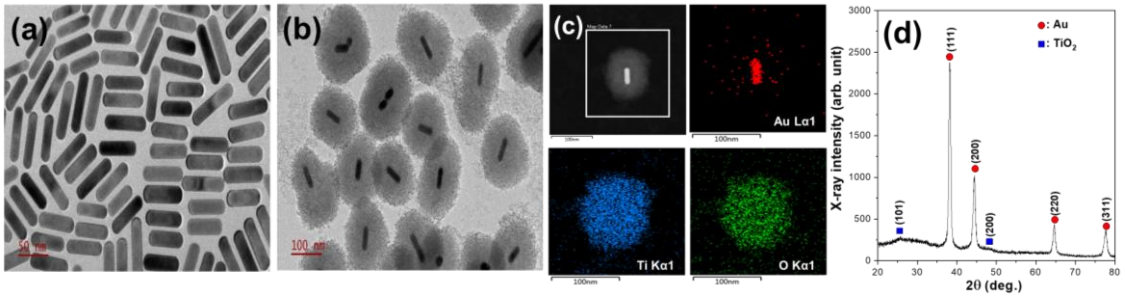

Figure 1. TEM images of (a) GNR and (b) GNR@TiO_2. (c) TEM-EDX images and (d) XRD pattern of GNR@TiO_2.

As shown in Fig. 1(c), TEM-EDX mapping images of the GNR@TiO_2 clearly confirm the uniform distribution of the TiO_2 shell surrounding the GNR core. The X-ray diffraction (XRD) patterns in Fig. 1(d) reveal characteristic peaks of face-centered cubic gold (JCPDS 04-0784) at 2θ = 38.1°, 44.4°, 64.6°, and 77.6° (highlighted by red circles). In contrast, two broad and weak XRD peaks of the GNR@TiO_2 at 25.5° and 48.2° (marked by a blue rectangle) suggest the presence of TiO_2 with poorly crystalline structure due to the absence of long-range order.

Recently, S. Choi et al. demonstrates that coating TiO_2 powder with tannic acid (TA) leads to an increased in UV blocking efficiency and a decreased photocatalytic effect[15]. Therefore, we utilized TA as a ROS scavenger for the GNR@TiO_2 as shwon in Fig. 2(a). The galloyl groups of TA readily facilitate chemical bonding to the TiO_2 surface through a ligand-to-metal

charge transfer (LMCT) mechanism. This enables the facile synthesis of TA-coated GNR@TiO_2 (TA-GNR@TiO_2) composites via simple stirring of a TA and GNR@TiO_2 composite solution.

Fig. 2(b) illustrates the zeta potential(ζ) variations of the TA-GNR@TiO_2 and its raw-materials. To coat the GNR surface with a TiO_2 layer, Ti^{3+} ions should be electrostatically bonded to the GNR surface. For this purpose, the cationic CTAB surfactant bonded to the GNR surface was substituted with the anionic SDS surfactant (ζ = -15.8 mV). As a result, the as-prepared GNR@TiO_2 exhibited a negative ζ of -5.7 mV. Additionally, when coated with TA(ζ= -19.5 mV), which was used as a reactive oxygen species scavenger, the ζ potential of TA-GNR@TiO_2 showed a strong negative ζ of -31.6 mV.

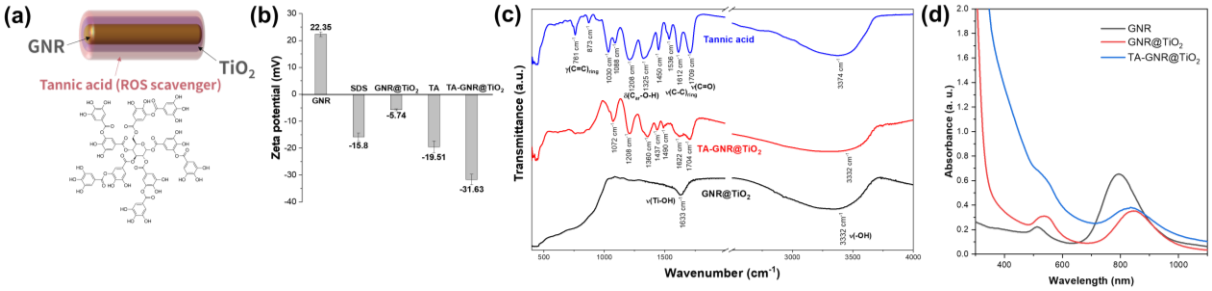

Figure 2. (a) Schematic illustration of TA-GNR@TiO_2 structure.(b) Zeta potential(ζ) variations of the TA-GNR@TiO_2 and its raw-materials. (c) FT-IR spectra of TA, GNR@TiO_2, and TA-GNR@TiO_2. (d) UV-Vis absorption spectra of GNR, GNR@TiO_2, and TA-GNR@TiO_2.

As shown in Fig. 2(c), the FT-IR spectrum of TA-GNR@TiO_2 revealed typical C=O streching vibration (ν(C=O)) at 1,704 cm^{-1}, aromatic C-C streching vibration ($\nu(C=C)_{ring}$) at 1,612 cm^{-1}, and C_{ar}-O-H in-plane bending vibration ($\delta(C_{ar}\text{-}O\text{-}H)$ at 1,208 cm^{-1} of tannic acid. This indicates successful tannic acid coating on the GNR@TiO_2 surface. In the UV-Vis absorption spectra presented in Fig. 2(d), the TA-GNR@TiO_2 shows increased absorption in the UV to visible light regions and a red-shift of the GNR's Longitudinal surface plasmon resonance wavelength (λ_{LSPR}) compared to the GNR due to the amorphous TiO_2 shell with a high refractive index (≥ 2.4) and the LMCT between TA and TiO_2. This suggests that TA-GNR@TiO_2 could be a promising material for blocking UV to IR-A light.

3.2 ROS scavenging efficiency of TA-GNR@TiO_2

Widely utilized as a UV blocking agent, TiO_2 is known as a inorganic particle with excellent photocatalytic effects. However, the ROS generated by this photocatalytic effect are harmful to the human body. As illustrated in Fig. 3(a), the formation of a Schottky junction between the gold and TiO_2 in GNR@TiO_2 prolongs the separation time of electrons and holes, consequently enhancing the photocatalytic effect. To verify whether the TA coating effectively blocks the ROS generated from GNR@TiO_2, a methylene blue(MB) degradation experiment was conducted. The MB readily changes color from blue to colorless through a reduction process, making it easy to observe the generation of ROS. Indeed, Fig. 3(b) shows that the mixed solution of GNR@TiO_2(30 ppm Au) and MB(10 ppm) became colorless upon increasing UV irradiation time. As shown in Fig. 3(c), the variation in MB concentration(10 ppm), analyzed *via* UV-Vis absorption spectroscopy, revealed that 60% of the MB was decomposed by GNR@TiO_2 after 3 hours of UV irradiation, compared to only 10% by TA-GNR@TiO_2. This indicates that the TA effectively scavenged the ROS generated from GNR@TiO_2.

Figure 3. (a) Schematic illustration of charge separation in Schottky junction of GNR@TiO_2 under UV-light irradiation. (b) Photos of MB degradation by GNR@TiO_2(30 ppm Au) aqueous solution as a function of UV-light irradiation time. (c) Variations of MB concentration(10 ppm) by GNR@TiO_2 and TA-GNR@TiO_2 solutions (30 ppm Au) upon UV-light irradiation time.

3.3 IR-A blocking in-vitro test for manufactured creams of GNRs, TiO_2, TA-GNR@TiO_2, and composites

The GNR@TiO_2 consists of an IR-A absorber (GNR core) coated with an IR-A scattering agent (TiO_2 shell). Therefore, it is expected that its IR-A blocking effect would be higher compared to the GNR alone. Actually, Fig. 4(a) and (b) clearly show that the upper region of the TA-GNR@TiO_2 solution (100 ppm Au) exhibits an intense glow due to significant IR-A scattering upon exposure to an IR-A laser(λ = 780 nm, spot size = 2 × 3 mm^2, power density = 1.2 W/cm^2), in contrast to the GNR solution (100 ppm Au).

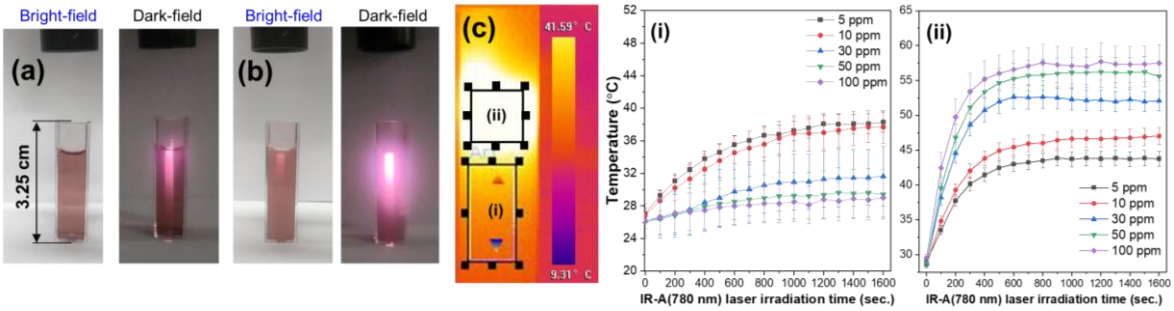

Figure 4. Bright-field and dark-field photos of (a) GNR and (b) TA-GNR@TiO_2 aqueous solutions with a concentration of 100 ppm Au under IR-A laser irradation. (c) IR-camera image and temperature variations in the lower *(i)* and the upper *(ii)* regions of TA-GNR@TiO_2 solution with increasing concentration (5 to 100 ppm Au).

As shown in Fig. 4(c), IR camera analysis of the TA-GNR@TiO_2 solution revealed that the temperature of the upper region (marked *(ii)*) was subsequently increased with increasing concentration (5 to 100 ppm Au) of TA-GNR@TiO_2 due to the enhanced photothermal effect. In contrast, the temperature of the lower region (marked *(i)*) decreased with increasing concentration of the TA-GNR@TiO_2 solution. Notably, the temperature decrease rate in the region *(i)* became prominent at concentrations of 30 ppm Au and above. This is attributed to the reduced transmittance of the IR-A laser in the region *(i)* as a result of the significantly increased IR-A scattering in the region *(ii)* by the TiO_2 shell of TA-GNR@TiO_2. Therefore, these results suggest that a sunscreen containing TA-GNR@TiO_2 is expected to provide a greater skin temperature reduction effect with increased IR-A blocking efficiency compared to a sunscreen containing GNR.

Fig. 5 present the temperature variations, ΔT (°C), and ΔTRI (%) values in the heating zone caused by the IR radiation passing through the slide-glass coated with creams containing vehicle, GNR, and TA-GNR@TiO_2 in which the TiO_2 concentration is set at 10^5 ppm but the GNR and TA-GNR@TiO_2 concentrations were varied from 0 to 500 ppm Au.

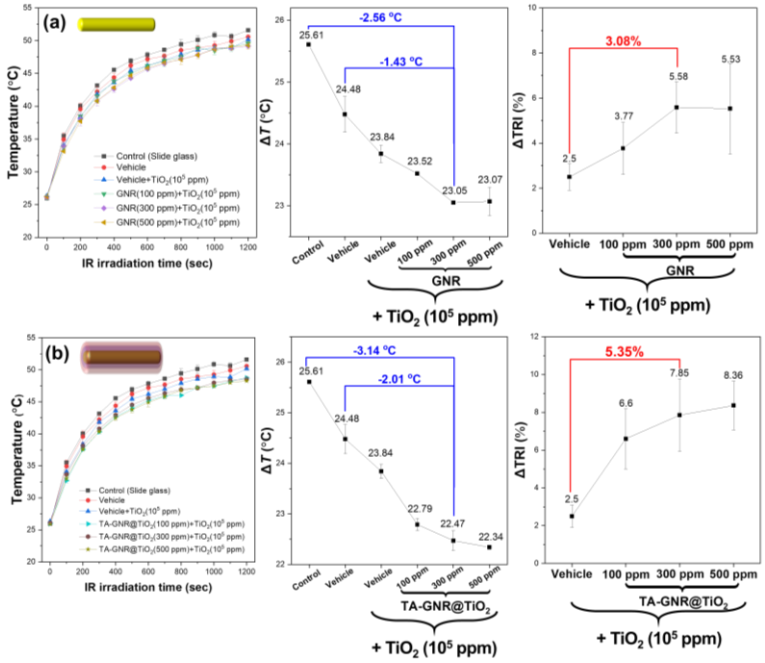

Figure 5. Variations in temperature, ΔT (°C), and ΔTRI (%) values of the heating zone exposed to IR radiation transmitted through slide-glasses coated with creams containing (a) GNR (0 ~ 500 ppm Au)/TiO_2 (10^5 ppm) and (b) TA-GNR@TiO_2 (0 ~ 500 ppm Au)/TiO_2 (10^5 ppm) mixed creams.

When the GNR concentration in the GNR/TiO_2 (10^5 ppm) mixed cream increased from 0 ppm to 300 ppm Au, the ΔT (°C) value decreased from 23.8 ± 0.2 °C to 23.1 ± 0.1 °C (Fig. 5(a)). Consequently, the ΔTRI (%) of the GNR(0 ~ 300 ppm Au)/TiO_2 (10^5 ppm) mixed cream linearly increased from 2.5 ± 0.6 % to 5.6 ± 1.1 % at the same concentration range (Fig. 5(a)). However, only slight changes in the ΔT (°C) and ΔTRI (%) values were observed at the GNR concentration exceeding 300 ppm. Notably, the ΔTRI (%) value of the TA-GNR@TiO_2 (300 ppm Au)/TiO_2 (10^5 ppm) mixed cream increased to 7.9 ± 1.9 %, which was 2.3% higher than that of the GNR (300 ppm Au)/TiO_2 (10^5 ppm) mixed cream(Fig. 5(b)). It is a consequence of the reduced ΔT (°C) of 22.5 ± 0.2 °C (Fig. 5(b)). The reason why the TA-GNR@TiO_2 composite exhibits superior ΔTRI (%) compared to GNR is that the TA-GNR@TiO_2 composite allows for the simultaneous occurrence of IR-A absorption and scattering within a single material.

3.4 Effect pf IR radiation on ROS generation in human fibroblast

A dose of 2 mg/cm^2 of the cream containing the vehicle or sample was applied to the lid of a culture dish containing the CCD-986sk human dermal fibroblasts. Subsequently, after approximately 10 min, the dish was irradiated with an IR lamp for 30 min. Fig. 6 presents the H_2DCFDA staining images of the CCD-986sk cells after exposure to IR radiation for 30 min using sample-coated glasses. The H_2DCFDA dye is commonly employed as an indicator of H_2O_2 cellular levels. Cellular ROS production was influenced by the IR radiation transmitted through various sample-coated glasses in the following order: slide-glass > vehicle > Vehicle/TiO_2(10^5 ppm) ≈ GNR(300 ppm Au) > TA-GNR@TiO_2(300 ppm Au) ≈ GNR(300 ppm Au)/ TiO_2(10^5 ppm) ≈ TA-GNR@TiO_2(300 ppm Au)/TiO_2(10^5 ppm).

Interestingly, the intracellular ROS fluorescence intensity generated by the IR light passing through the slide glass applied with TA-GNR@TiO_2(300 ppm Au) cream was similar to that of the GNR (300 ppm Au)/TiO_2 (10^5 ppm) and TA-GNR@TiO_2 (300 ppm Au)/TiO_2 (10^5 ppm) mixed creams. This is likely attributed to the exceptionally high IR-A blocking efficiency of TA-GNR@TiO_2.

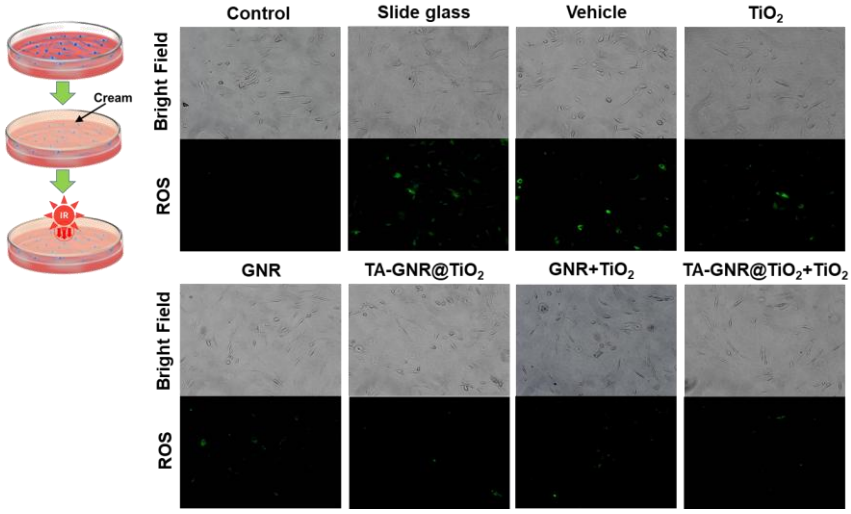

Figure 6. Bright-field and ROS fluorescence confocal images of the CCD-986sk cells after 30 min of IR irradiation transmitted through different samples: slide-glass (control), vehicle, TiO_2 (10^5 ppm), GNR (300 ppm Au), TA-GNR@TiO_2 (300 ppm Au), GNR (300 ppm Au)/TiO_2 (10^5 ppm), and TA-GNR@TiO_2 (300 ppm Au)/TiO_2 (10^5 ppm) cream-coated glass.

3.5 Clinical results

Fig. 7 illustrates the changes in skin temperature and the corresponding ΔTRI (%) values calculated after applying creams containing the GNR (300 ppm Au)/TiO_2 (10^5 ppm) and the TA-GNR@TiO_2 (300 ppm Au)/TiO_2 (10^5 ppm) to the dorsal skin of 40 clinical participants at a dose of 2 mg/cm², followed by 10 minutes of IR irradiation. Application of cream containing the GNR (300 ppm Au)/TiO_2 (10^5 ppm) resulted in a decrease in skin temperature of –1.5 ± 1.3 °C compared to the control (no cream applied) and –1.3 ± 1.3 °C relative to the vehicle cream. In contrast, the cream containing the TA-GNR@TiO_2 (300 ppm Au)/TiO_2 (10^5 ppm) led to a more pronounced decrease in skin temperature of –2.3 ± 1.1 °C and –2.1 ± 1.0 °C, respectively.

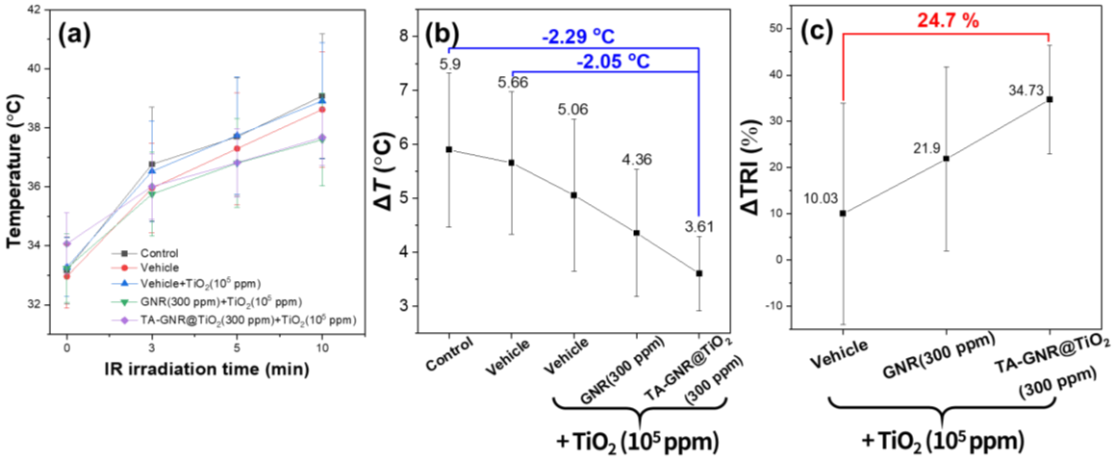

Figure 7. Results from a clinical study involving 40 participants; Changes in (a) skin temperature, (b) ΔT, and (c) ΔTRI (%) after 10 minutes of IR irradiation on the skin areas treated with no cream (control), vehicle, vehicle/TiO_2 (10^5 ppm), GNR (300 ppm Au)/TiO_2 (10^5 ppm), and TA-GNR@TiO_2 (300 ppm Au)/TiO_2 (10^5 ppm) creams.

Based on these results, the calculated ΔTRI (%) values were 10.0% for the vehicle/TiO_2 (10^5 ppm) cream, 21.9 % for the GNR (300 ppm Au)/ TiO_2 (10^5 ppm) cream, and 34.7 % for the TA-GNR@TiO_2 (300 ppm Au)/TiO_2 (10^5 ppm) cream. These findings suggest that

incorporation of the GNR (300 ppm Au) into the TiO_2 (10^5 ppm)-based sunscreen formulation enhanced the ΔTRI (%) by 11.9 %, while addition of the TA-GNR@TiO_2 (300 ppm Au) resulted in a 24.7 % increase. Notably, the TA-GNR@TiO_2 (300 ppm Au) formulation demonstrated approximately a twofold improvement in thermal blocking efficiency compared to the GNR (300 ppm Au) formulation.

4. Conclusion

In this study, the GNR@TiO_2 composite was successfully synthesized by combining the GNR as IR-A absorbers with TiO_2 as IR-A scattering agent. To suppress the generation of the ROS caused by the photocatalytic activity of the GNR@TiO_2, the composite was further coated with the tannic acid (TA), resulting in the formation of the TA-GNR@TiO_2. Photodegradation experiments using methylene blue confirmed that the TA effectively scavenges ROS. In vitro experiments demonstrated that the cream formulation containing the TA-GNR@TiO_2 composite exhibited superior thermal blocking efficiency compared to the GNR-based formulation and also reduced intracellular ROS production. Clinical trial results further confirmed that the TA-GNR@TiO_2 formulation provided more than twice the thermal blocking efficiency compared to the GNR formulation. As global warming accelerates and summer seasons become longer, there is an increasing demand for sunscreens that can protect not only against UV radiation but also prevent thermal aging caused by IR-A radiation. The micro-sized TA-GNR@TiO_2 composite is therefore considered a promising candidate for the development of next-generation IR-A blocking agents.

5. Acknowledgments

This research was supported by the Korean Ministry of Education, Science, and Technology (grant number : 2016R1D1A3B0201175615, 10%), the Korea Health Technology R&D Project (grant number : HP23C0260, 70%) through the Korea Health Industry Development Institute (KHIDI) supervised by the Ministry of Health and Welfare, and Innovative Human Resource Development for Local Intellectualization Support Program (grant number : IITP-2025-RS-2020-II201612, 20%) supervised by the Institute of Information & Communications Technology Planning & Evaluation(IITP).

6. References

[1] W. Müller et al. (Editor), *Springer Nature*, 17-32, **2022**
[2] Gerard Mcknight et al., *Surgery (Oxford)*, 40(1), 8-12, **2022**
[3] Amy H.Huang et al. *Current Dermatology Reports*, 9, 22-29, **2020**
[4] Tiina I. Karu, *IUBMB Life*, 62(8), 607-610, **2010**
[5] Claudia Dompe et al., *Clinical Medicine*, 9(6), 1724, **2020**
[6] P. Schroeder et al., *J. Invest. Dermatology*, 128, 2491-2497, **2008**
[7] S. Shimizu et al., *Photochemistry and Photobiology*, 96(5), 1105-1115, **2020**
[8] Chris S. Ivanoff et al., *Food and Chemical Toxicology*, 50(2), 212-215, **2012**
[9] S. Sundar et al., *J. Environmental Research and Public Health*, 7(12), 4267-4277, **2010**
[10] X. Yang et al., *Chemical Reviews*, 115(19), 10410-10488, **2015**
[11] Bo-Mi Kim et al., *BKCS*, 37(6), 931-937, **2016**
[12] B. Nikoobakht et al., *Chemistry of Materials*, 15(10), 1957-1962, **2003**
[13] Jonathan G. Mehtala et al., *Langmuir*, Vol 30, Issue 46, 13727-13730, **2014**
[14] K. R. Lee et al., Korea patent, 10-1595565, **2016**
[15] Saehan Choi et al., *ACS Applied Material & Interfaces*, 16(13), 16767-16777, **2024**